coatings

MDPI

Article

High-Entropy Alloy Coating Produced by Laser Metal Deposition with Additional Femtosecond Laser Surface Structuring

Márk Windisch [1,2], Gergely Juhász [1,3,4], Anita Heczel [1], József T. Szabó [1], Zoltán Dankházi [2] and Ádám Vida [1,*]

[1] Bay Zoltán Nonprofit Ltd. for Applied Research, Kondorfa Street 1, 1116 Budapest, Hungary; mark.windisch@bayzoltan.hu (M.W.); gergely.juhasz@bayzoltan.hu (G.J.); heczel.anita@gmail.com (A.H.); jozsef.szabo@bayzoltan.hu (J.T.S.)
[2] Department of Materials Physics, Eötvös Loránd University, Pázmány Péter Promenade 1/A, 1117 Budapest, Hungary; zoltan.dankhazi@ttk.elte.hu
[3] Department of Innovative Vehicles and Materials, GAMF Faculty of Engineering and Computer Science, John Von Neumann University, Izsáki Street 10, 6000 Kecskemét, Hungary
[4] Doctoral School on Materials Sciences and Technologies, Óbuda University, Népszínház Street 8, 1081 Budapest, Hungary
* Correspondence: adam.vida@bayzoltan.hu; Tel.: +36-70-515-7182

Abstract

High-entropy alloys (HEAs) represent one of the most promising emerging material families, particularly for advanced surface engineering applications. In this work, a near-high-entropy alloy (near-HEA) coating was produced on a 316L stainless steel substrate using laser metal deposition (LMD) from a powder mixture of Inconel 625, Cr and Mo, without the intentional addition of Fe. Due to dilution from the substrate, the resulting alloy contained elevated Fe content while maintaining Cr, Ni and Mo concentrations within the generally accepted compositional range of HEAs. The deposited layer exhibited a dual-phase microstructure consisting of a face-centered cubic (FCC) phase and a highly distorted tetragonal phase forming a periodic network with a characteristic length scale of several hundred nanometers. The hardness of the coating increased to approximately three times that of the substrate, reaching values of 600–700 HV. To further modify the surface properties, laser-induced periodic surface structures (LIPSS) were generated on the polished coating using femtosecond pulsed laser irradiation at different energy densities. The morphology and subsurface structure of the resulting periodic patterns were investigated by scanning electron microscopy. LIPSS with characteristic dimensions ranging from the micrometer to nanometer scale were successfully produced. Cross-sectional analyses revealed that the underlying dual-phase microstructure remained continuous within the laser-structured regions, indicating that LIPSS formation occurred predominantly via metallic ablation without significant phase transformation or amorphization. These results demonstrate the combined applicability of LMD and femtosecond laser structuring for producing mechanically enhanced, micro- and nanostructured near-HEA coatings with potential for advanced surface-related functionalities.

Keywords: HEA; LIPSS; LMD; femtosecond laser surface modification

Academic Editor: Yanxin Qiao

Received: 4 January 2026
Revised: 30 January 2026
Accepted: 3 February 2026
Published: 6 February 2026

1. Introduction

The history of metallic coatings dates back 3–4 millennia to BC, when bronze plates were hammered with gold leaf. From these initial methods, metallic coating expanded in the 20th century when numerous new physical and chemical methods became available in addition to the previously known galvanic layer deposition [1]. Examples include vacuum evaporation, magnetron sputtering and atomic layer deposition (ALD) [2–4]. These modern methods make it possible to deposit metallic layers on metallic and non-metallic substrates ranging in thickness from nano to several micrometers. Depositing layers in a specific way (size, multi-layer) can tune the physical properties of these surfaces, such as their optical, mechanical, electrical or corrosion properties. Several modern techniques can be used to achieve coated layers with a thickness ranging from tens to hundreds of micrometers [5–7]. One of these is laser metal deposition (LMD), which can be used to apply alloy layers to metal substrates. Using the LMD technique, layers with a specific composition and structure can be applied by using the appropriate metal powders and laser treatment [8,9]. A newer area of LMD research involves forming high-entropy alloy (HEA) layers, which can significantly enhance the substrate's physical and chemical properties [10–12]. Numerous near-HEAs and HEAs can be created by utilizing the heat treatment associated with chemical mixing provided by LMD. This includes various processing conditions, such as heating and cooling, which can achieve new metastable states. This enables the development of a wide range of mechanical properties.

In recent years, Li et al. have compiled a summary of HEAs created with LMD and their main properties [13]. Based on this, previous work has mainly focused on producing CrCoFe-containing HEA layers with LMD [14–16]. The formed layers exhibit advantageous properties in terms of hardness, strength, toughness, and wear resistance. The higher hardness values result from lattice distortion and, in many cases, from the fine grain structure that has been formed. The strength is related to the second phase that appears in HEAs, while the improved wear resistance can be explained not only by the hardness but also by the microstructure that has been formed. There are numerous definitions and explanations for HEAs and their properties [17,18]. The basic idea of HEA was formulated by Gou, among others, who determined the mixing enthalpy to be between −7 and 22 kJ/mol and the mixing entropy to be between 11 and 19.5 J/(K·mol) [19]. In addition to the quantitative formulation, HEA as a created solid solution is defined by four main properties: high mixing entropy, severe lattice distortion, sluggish diffusion, and the "cocktail" effect. These factors all contribute to the final physical properties of the resulting alloy. It is important to note at this point that the formed alloy by a given production process may also be in a metastable state, resulting in some possible variety of new properties [20]. This potential property offering of HEAs inspired the production of HEA layers using LMD and their further surface modification.

There are a number of traditional physical and chemical surface treatments that can be used to further improve the surface properties of coatings, e.g., chemical etching, surface heat treatment or mechanical scribing. In addition, there are a number of other modern ion beam, plasma-based, and laser surface treatments. Depending on the properties of the laser beam, laser machining can remove or melt material, or even structure the surface at scales ranging from micrometers to several millimeters. Laser surface treatments, including femtosecond pulse laser treatment, are suitable for structuring surfaces at micrometer and sub-micrometer scales [21]. These surface structures can improve the optical, wetting or tribological properties of coatings [22–27]. In addition, surface treatments can be performed on areas as small as a few tens of square micrometers, which opens up further potential for industrial applications.

In our previous work, we demonstrated the feasibility of producing high-entropy alloy layers by LMD using separate elemental powders without pre-alloying [28]. Building on these results, the present study aims to fabricate a near-HEA coating on a 316L stainless steel substrate using Inconel 625 combined with Cr and Mo powders, while explicitly accounting for compositional modification due to substrate dilution.

In addition to microstructural and phase analysis of the deposited layer, a further objective of this work is to investigate the formation of laser-induced periodic surface structures on this complex, multi-phase alloy using femtosecond laser irradiation. Special emphasis is placed on assessing whether the characteristic dual-phase microstructure remains stable during ultrafast laser processing, as no prior studies have addressed LIPSS formation on HEA or near-HEA systems.

2. Materials and Methods

During laser metal deposition, Inconel625 (m4p Ni-625, Advanced Metal Powders, Mumbai, MA, USA), Cr (99+%, Thermo Scientific, Waltham, MA, USA), and Mo (99.95%, Thermo Scientific, Waltham, MA, USA) metal powders on the 316L stainless steel substrate were used with average particle sizes of 43 µm, 50 µm, and 53 µm, respectively. The powder mixture used (60 wt% Inconel 625—20 wt% Cr—20 wt% Mo). The element composition of the mixture powder for the main component is contained in Table 1.

Table 1. The average element composition of the mixture of Inconel625, Cr and Mo powder.

Mixture Powder	Atom%	Weight%
Chromium	39.8	33
Nickel	38.6	36.3
Molybdenum	16.7	25.5
Iron	3.4	3
Niobium	1.5	2.2

The powder mixture was fed into a GTV PF 2/2 LC powder feeder (GTV, Luckenbach, Germany), with 4.6 argon applied as the carrier gas for the powder dispersion. Before the laser processing, due to removing surface oxide layer, the surface of the 316L stainless steel substrate was ground using P320 SiC paper and after which it was washed with ethanol. Laser metal deposition was performed using a Trumpf TruLaser Cell 7020 with a true disk laser source equipped with a dual-core fiber optic cable (Trumpf SE + Co. KG, Ditzingen, Germany). The laser machine was also supplemented with a CNC-controlled laser processing device for movement control. During the laser construction of the metal layer, based on our previous work and other studies, the laser beam spot size was 4 mm, the power was 1500 W, and the scanning speed was 0.8 m/min [28–30]. The laser deposition powder feeder disk speed was 3 rpm, while the carrier gas flow rate was 4 L/min. The laser scanning strategy was zigzag with 60% overlap. We kept in mind that the powders and their carriers should melt, but at the same time, the mixing of the base material should not significantly affect the elemental composition of the desired coating. The laser metal deposition was performed on 10 mm-thick 316 L stainless steel with a base area of 100 mm × 100 mm at atmospheric pressure.

A TESCAN VEGA 4 (Tescan Group a.s., Brno, Czech Republic) scanning electron microscope (SEM) equipped with an energy dispersive X-ray (EDX) detector was used for the microscopic and element composition examination of the built layer. The error for the elemental compositions obtained during EDX measurements (see Tables 1 and 2) is estimated to be between 0.2 and 1 at%. Material structure was investigated using an Oxford Symmetry S3 (Oxford Instruments, Abingdon, UK) electron backscatter diffraction

detector supplemented by five forward scattered electron detectors (FSD), connected to a JEOL IT700HR-LA (JEOL, Tokyo, Japan) SEM.

Table 2. Cross-section elemental composition of the created metal layer on the 316L substrate.

Mixture Powder	Atom%	Weight%
Iron	45	43
Chromium	26.5	23.6
Nickel	19.2	19.3
Molybdenum	7.2	11.7
Manganese	1.4	1.3
Niobium	0.7	1.1

The hardness of the layer was measured using an Anton Paar MHT-4 (Anton Paar, Graz, Austria) Microhardness tester equipped with a Leica MEF4M (Leica Microsystems, Wetzlar, Germany) optical microscope. Microhardness measurements were performed on the polished cross-sectional of the layer built with LMD, with increments of approximately 60 μm.

The phase composition of the investigated samples was analyzed by X-ray diffraction (XRD). Measurements were performed using a Rigaku Miniflex II (Rigaku, Tokyo, Japan) powder diffractometer operated at 30 kV and 15 mA, employing CuKα radiation with a wavelength of λ = 0.15418 nm. The obtained diffraction patterns revealed the presence of both face-centered cubic (FCC) and tetragonal phases in all samples. The average lattice parameter of the FCC phase was calculated from the diffraction peak positions using the Nelson–Riley extrapolation method [31]. Identification of the tetragonal phase was conducted with the PDF-5+ database, applying the search–match algorithm. This algorithm systematically compares the peak positions and relative intensities of the experimental data with reference entries in the database, subsequently ranking candidate phases and suggesting the most probable matches.

The surface structuring of the built metal layer was performed using a femtosecond laser equipment with a Coherent Monaco 1035 (Coherent Corp., Saxonburg, PA, USA) Nd:YAG laser source. The laser pulse duration can be adjusted between 277 fs and 10 ps, with a maximum energy of 60 W. The repetition rate can be adjusted between 188 kHz and 50 MHz, with a maximum pulse energy between 80 μJ and 1.2 μJ. The femtosecond laser system was supplemented with a 254 mm focal length F-theta lens containing Scanlab Scancube III 14 (Scanlab GmbH, Puchheim, Germany) scanning optics which provides the movement of the laser beam. The Femtosecond laser surface treatments were performed at repetition frequencies of 1 MHz, with different pulse energies and scanning speeds at room temperature under atmospheric conditions.

3. Results

The cross-sectional image of the around 1 mm thick layer deposited on the 316L substrate is shown in Figure 1. The mixture resulting from the Marangoni convection can be observed in SEM image as in previous laser deposition studies.

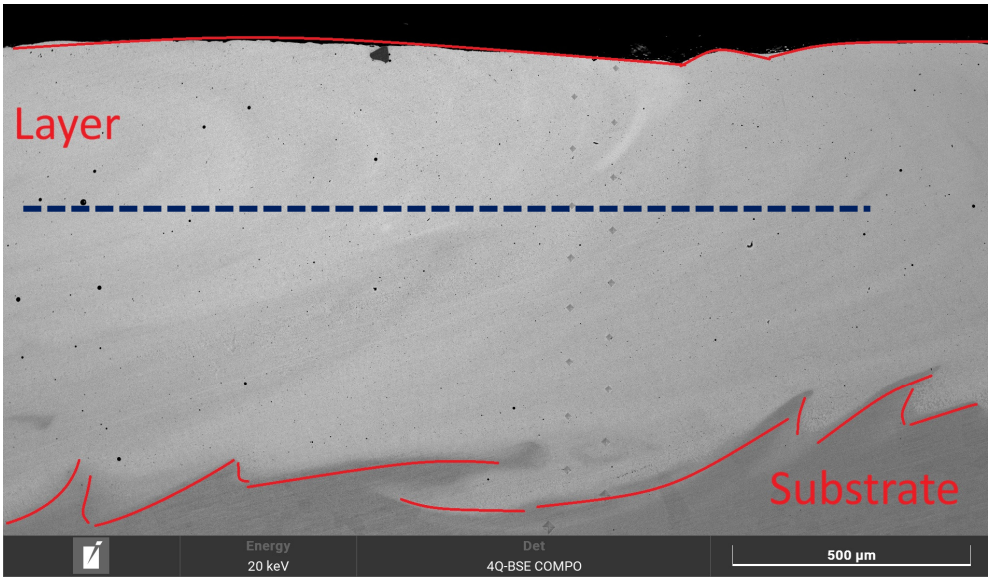

Figure 1. The cross-section of the created metal layer built by laser metal deposition. The position of the back grinding is marked with a blue dashed line.

The significant mixing is well illustrated by the fact that, apart from the 100–200 µm transition zone, according to the areas EDX measurements, the iron content originating from the substrate shows homogeneously distributed within a few atomic percent. The elemental composition of the built layer is shown in Table 2.

The hardness values at the cross-section of the layer were measured between 550 HV and 750 HV, except for a section of approximately 100–200 µm where a rapid increase in hardness was observed (Figure 2).

For the material structure analysis and surface modification, the layer was ground down to around 300 µm (blue dashed line in Figure 1) with P800, P1200, and P2500 SiC paper and finally polished with 3 µm, 1 µm Microdiamant diamond suspension, and a 40 nm Stuers OP-U silica suspension. After polishing, the sample was rinsed with ethanol and distilled water. X-ray diffraction measurements were performed on the prepared sample surface to determine the phases of the layer (Figure 3).

According to XRD measurements, two phases can be observed in the layer: a face-centered cubic, FCC, (No. 225 F/m-3 space group) and a tetragonal crystal (No. 136 P42/mnm) structure, with lattice constants of a = 0.3613 nm and a = 0.8854 nm, c = 0.4607 nm, respectively. Based on the forescatter electron detector (FSD) image of the polished surface of the layer, the two phases are mostly located in a street-like network of ~100–150 nm (Figure 4). The EDX measurements demonstrate an increase in nickel and chromium–molybdenum concentration in the dark (tetragonal) and light (FCC) phases, respectively.

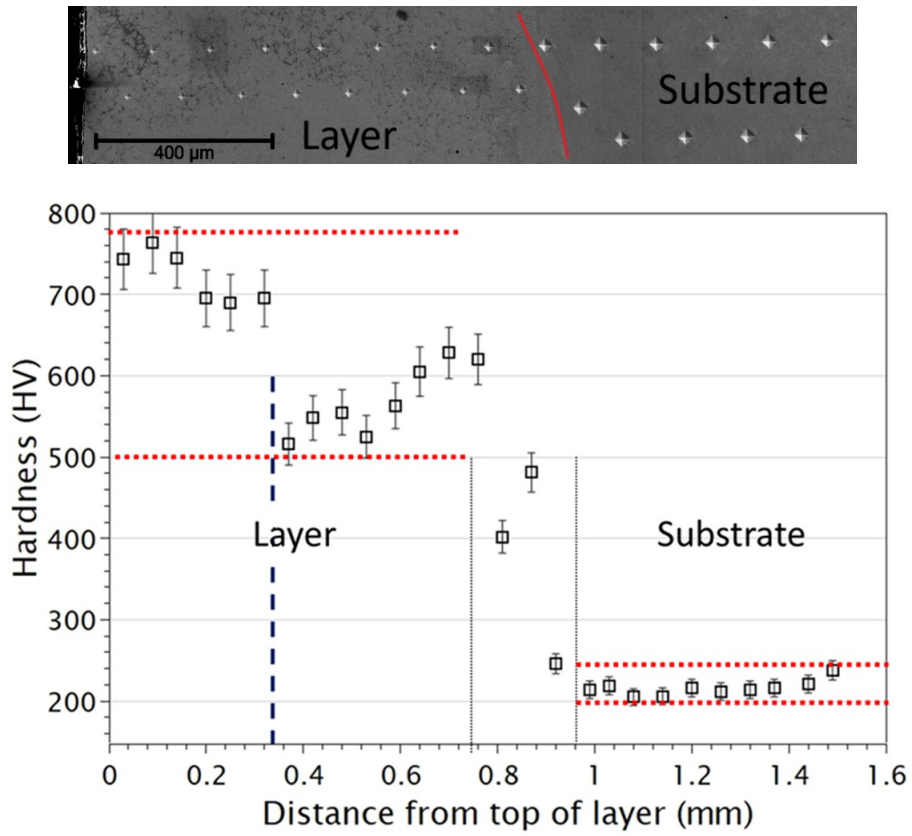

Figure 2. The measured hardness values of the created layer (see the indentation in the SEM image above the graph-a red line marks the boundary between the layer and the substrate) as a function of the distance from the top of the layer. The range of hardness values characteristic of the layer and substrate and the position of the grinding: red dotted and blue dashed line in the graph.

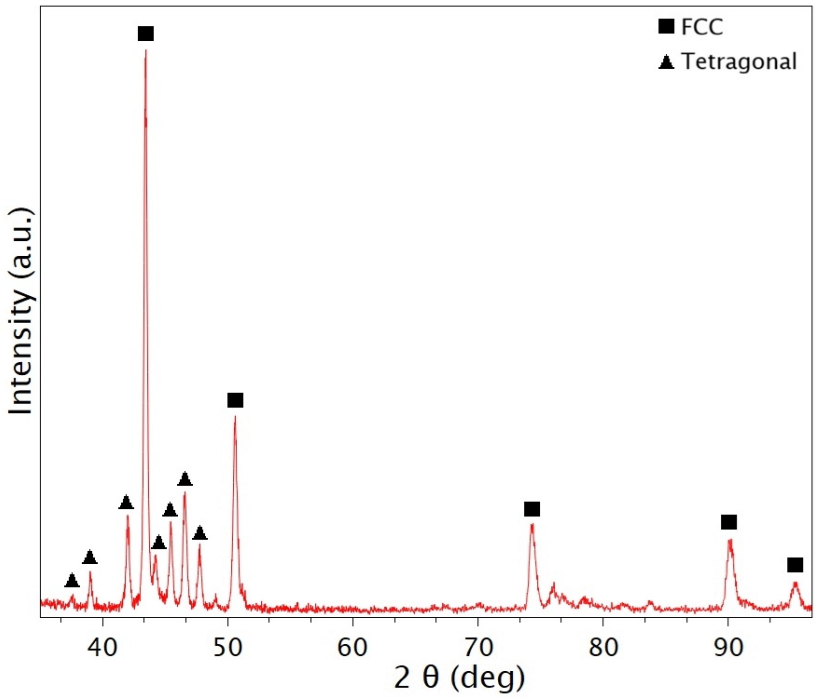

Figure 3. XRD measurements of the created metal layer. The FCC and tetragonal phase peaks are marked as squares and triangles, respectively.

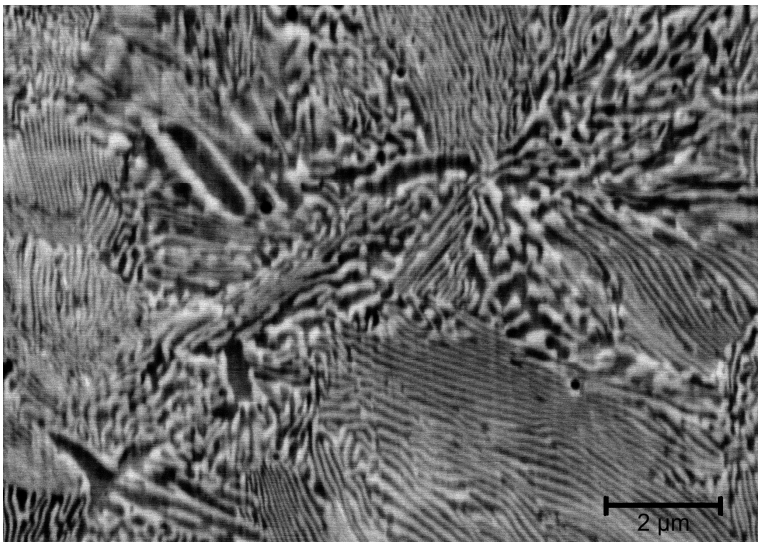

Figure 4. FSD image of the polished layer, showing the tetragonal phase as dark and the FCC phase as light.

The polished surface of the layer was structured using a femtosecond pulsed laser machining with a pulse duration of 277 fs. The laser surface treatment was performed at four different energy densities, i.e., different pulse energies and scanning speeds (Figure 5).

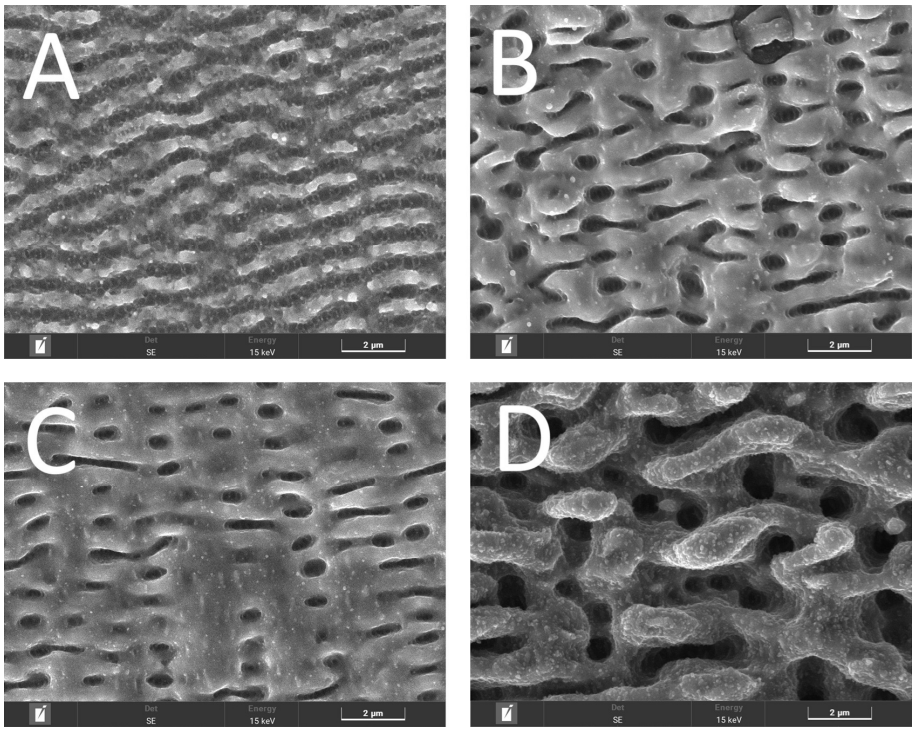

Figure 5. Morphology of surface periodic structures formed by femtosecond laser surface treatments at different energy densities ((**A**): 6 J/cm^2, 30 µJ, 10 m/s; (**B**): 30 J/cm^2, 18 µJ, 1 m/s; (**C**): 90 J/cm^2, 60 µJ, 1 m/s; (**D**): 300 J/cm^2, 12 µJ, 0.1 m/s).

Surface structure in Figure 5A contains LIPSS with a regular periodicity of ~1 µm and a depth of 100 nm, caused by several overlaps of laser pulses, with a few spherical units measuring 10–200 nm. The surface structures marked in Figure 5B,C contain units measuring 1–2 µm and pits measuring 10–200 nm. In the case of Figure 5D, due to the

increased energy input, significant material removal occurs, and oxide-rich particles in the order of tens of nanometers appear.

In order to gather information about the processes inside LIPSS, FSD images of the result were taken from a newer cross-section (Figure 6). Based on the FSD images, the two separate phase regions beneath the laser-treated areas appeared in all cases as a continuous region without interruption within the LIPSS. The results obtained do not suggest any phase mixing or formation of an amorphous layer.

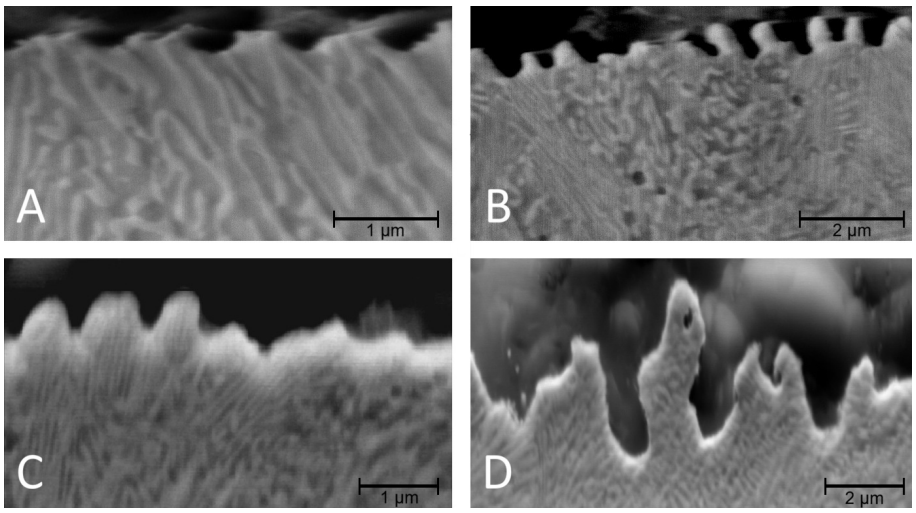

Figure 6. Cross-sectional FSD image of the surface structures shown in Figure 5. ((**A**): 6 J/cm^2, 30 µJ, 10 m/s; (**B**): 30 J/cm^2, 18 µJ, 1 m/s; (**C**): 90 J/cm^2, 60 µJ, 1 m/s; (**D**): 300 J/cm^2, 12 µJ, 0.1 m/s).

4. Discussion

4.1. Phase Constitution and HEA Characteristics

One of the primary objectives of this study was to produce a high-entropy-type coating by LMD using Inconel 625, Cr and Mo powders on a 316L stainless steel substrate, without the direct addition of iron powder. While the atomic concentrations of Cr, Ni and Mo in the deposited layer fall within the commonly accepted 5–35 at. % range for HEAs, the Fe content exceeds this limit due to dilution from the substrate. This is reflected in the calculated configurational entropy of mixing (11.8 J·mol^{-1}·K^{-1}), which approaches but does not fully reach the conventional HEA threshold of 1.5R, justifying the classification of the material as a near-high-entropy alloy.

Based on the calculated valence electron concentration (VEC = 7–8), the literature would typically predict the formation of an FCC + BCC dual-phase structure. In contrast, experimental results revealed the presence of an FCC phase accompanied by a tetragonal crystal structure, which is rarely reported in HEA systems [32]. This deviation can be attributed to the highly non-equilibrium solidification conditions inherent to the LMD process, including rapid cooling rates, steep thermal gradients, and local compositional fluctuations. The pronounced lattice distortion of the tetragonal phase, characterized by a c/a ratio of approximately 0.52, suggests a strongly compressed crystal structure consistent with one of the fundamental strengthening mechanisms of HEAs. The significantly increased hardness of the coating is therefore primarily attributed to this distorted phase, where dislocation motion is strongly impeded due to elevated lattice friction stresses.

Based on our XRD measurements, the tetragonal phase of the produced HEA is consistent with the lattice constant values and ratios of the σ phase with the VCrMnFeCoNi composition mentioned in Gorban's work [33]. Furthermore, the calculated VEC value of 7.67 indicates an FCC + tetragonal structure, which matches our produced phase. Gorban assumes that a BCC to tetragonal phase transition occurs during evolution, primarily in

response to changes in the temperature gradient. In this case, this occurs by facilitating the processes that take place during laser melting.

4.2. LIPSS Formation and Microstructural Stability

Femtosecond laser surface structuring was applied with a pulse duration of 277 fs to minimize heat-affected zones and suppress conventional melting-driven surface modification. At higher applied energy densities (samples A–D in Figure 5), surface features indicative of rapid material removal and resolidification were observed. In other words, during LIPSS formation at this energy density, laser ablation is governed by ultrafast non-equilibrium electron excitation and spatially modulated energy deposition. This leads to periodic material removal and redeposition. This raises the question of whether the characteristic dual-phase microstructure of the near-HEA coating remains stable within the LIPSS-modified regions.

Cross-sectional FSD analyses revealed that, regardless of the applied energy density, the FCC and tetragonal phases remain continuous beneath the laser-structured surface. No evidence of phase mixing, amorphization, or microstructural disruption was detected. These observations indicate that LIPSS formation on the investigated near-HEA coating occurs predominantly via ultrafast metallic ablation, governed by electron–phonon decoupling and highly localized energy deposition typical of femtosecond laser–matter interaction.

To the authors' knowledge, this work represents the first systematic investigation of LIPSS formation on a near-high-entropy alloy system. Consequently, the conclusions drawn here are based on direct experimental evidence rather than the established literature precedent.

5. Summary

Our current work had two main goals: to create a HEA layer using Inconel625, Cr, and Mo powder with an atomic percentage close to that of the four main components on a 316L stainless steel substrate. To achieve the strictly accepted HEA layer, further development requires one to optimize the laser (power and scanning speed) and powder feeding parameters (quantity, ratios, etc.). The other aim was to create LIPSSs on a created layer using a femtosecond laser, examine their morphology, and make assumptions about their formation mechanism. In the other case, based on the tests performed on LIPSS, they were mainly formed through an ablation process. During the first part of our work, a near-HEA coating was created, which resulted in a material with an FCC + tetragonal structure that is rare in the literature. We achieved a significant increase in hardness (over 600 HV) due to the tetragonal phase of the two-phase coating and its fine distribution in the FCC. In the second part of our work, we structured the surface of the existing coating at the micro- and nanoscale using a femtosecond pulse laser. During the cross-sectional examination of the formed structures, we found that no phase mixing occurred in the two-phase material of the coating. This finding also supports the assumption of metallic ablation during the formation of periodic structures. The observed surface morphologies and preserved subsurface microstructure suggest potential improvements in surface-related properties such as wear resistance, friction behavior, and functional wettability. Future work will focus on systematic tribological investigations to quantify these effects.

Summarizing our work, creating the HEA layer using LMD was to demonstrate that we can produce a HEA coating with further potential in terms of materials science and application in an industrially understandable environment. This means that there is a large sample size and no special atmosphere. We presented the initial experimental results of our research into femtosecond pulse laser processing, demonstrating surface

nanostructuring in specific areas of up to a few tens of micrometers. Also focusing on industrial applications, we examined the targeted structuring of microcomponents and other surfaces on the micrometer scale.

Author Contributions: M.W.: conceptualization, writing—original draft preparation, writing—review and editing, investigation, visualization, formal analysis. G.J.: methodology. A.H.: investigation, visualization. J.T.S.: investigation. Z.D.: writing—review and editing, formal analysis. Á.V.: writing—review and editing, supervisor. All authors have read and agreed to the published version of the manuscript.

Funding: The project is supported by the Chips Joint Undertaking and its member Hungary. Supported by the KDP-2021 Program of the Ministry of Innovation and Technology from the source of the National Research, Development and Innovation Fund.

Data Availability Statement: The data that support the findings of this study are all own results of the authors, not available anywhere.

Conflicts of Interest: Author Márk Windisch, Anita Heczel, József T. Szabó, Gergely Juhász and Ádám Vida were employed by the company Bay Zoltán Nonprofit Ltd. for Applied Research. The remaining authors declare that the research was conducted in the absence of any commercial or financial relationships that could be construed as a potential conflict of interest.

References

1. Galedari, S.A.; Mahdavi, A.; Azarmi, F.; Huang, Y.; McDonald, A. A Comprehensive Review of Corrosion Resistance of Thermally-Sprayed and Thermally-Diffused Protective Coatings on Steel Structures. *J. Therm. Spray Technol.* **2019**, *28*, 645–677. [CrossRef]
2. Borowski, P.; Myśliwiec, J. Recent Advances in Magnetron Sputtering: From Fundamentals to Industrial Applications. *Coatings* **2025**, *15*, 922. [CrossRef]
3. Johnson, R.W.; Hultqvist, A.; Bent, S.F. A Brief Review of Atomic Layer Deposition: From Fundamentals to Applications. *Mater. Today* **2014**, *17*, 236–246. [CrossRef]
4. Baptista, A.; Silva, F.; Porteiro, J.; Míguez, J.; Pinto, G. Sputtering Physical Vapour Deposition (PVD) Coatings: A Critical Review on Process Improvement and Market Trend Demands. *Coatings* **2018**, *8*, 402. [CrossRef]
5. Deng, Y.; Chen, W.; Li, B.; Wang, C.; Kuang, T.; Li, Y. Physical Vapor Deposition Technology for Coated Cutting Tools: A Review. *Ceram. Int.* **2020**, *46*, 18373–18390. [CrossRef]
6. Freund, L.B.; Suresh, S. *Thin Film Materials: Stress, Defect Formation and Surface Evolution*; Cambridge University Press: Cambridge, UK, 2004. [CrossRef]
7. Abegunde, O.O.; Akinlabi, E.T.; Oladijo, O.P.; Akinlabi, S.; Ude, A.U. Overview of Thin Film Deposition Techniques. *AIMS Mater. Sci.* **2019**, *6*, 174–199. [CrossRef]
8. Ghasempour-Mouziraji, M.; Lagarinhos, J.; Afonso, D.; Alves de Sousa, R. A Review Study on Metal Powder Materials and Processing Parameters in Laser Metaleposition. *Opt. Laser Technol.* **2024**, *170*, 110226. [CrossRef]
9. John Solomon, I.; Sevvel, P.; Gunasekaran, J.; Tanushkumaar, P. A Review on Additive Manufacturing of Alloys Using Laser Metal Deposition. *Mater. Today Proc.* **2022**, *64*, 44–50. [CrossRef]
10. Gong, N.; Meng, T.L.; Cao, J.; Wang, Y.; Karyappa, R.; Ivan Tan, C.K.; Suwardi, A.; Zhu, Q.; Ngo, A.C.Y.; Misra, K.P.; et al. Laser-Cladding of High Entropy Alloy Coatings: An Overview. *Mater. Technol.* **2023**, *38*, 2151696. [CrossRef]
11. Piglione, A.; Dovgyy, B.; Liu, C.; Gourlay, C.M.; Hooper, P.A.; Pham, M.S. Printability and Microstructure of the CoCrFeMnNi High-Entropy Alloy Fabricated by Laser Powder Bed Fusion. *Mater. Lett.* **2018**, *224*, 22–25. [CrossRef]
12. Chen, S.; Tong, Y.; Liaw, P.K. Additive Manufacturing of High-Entropy Alloys: A Review. *Entropy* **2018**, *20*, 937. [CrossRef] [PubMed]
13. Li, Y.; Shi, Y.; Wang, S. A Review of Microstructures and Properties of High-Entropy Alloys Manufactured by Laser Metal Deposition. *JOM* **2025**, *77*, 7093–7110. [CrossRef]
14. Huang, L.; Li, R.; Sun, Y.; Guan, D.; Liang, C.; Jiang, C.; Chen, J.; Wang, D.; Li, J. A Solution to the Hot Cracking Problem and Anisotropic Mechanical Properties for Directed Energy Deposition FeCoNiCr Multi-Principal-Element Alloy. *Metals* **2022**, *12*, 1581. [CrossRef]
15. Dada, M.; Popoola, P.; Mathe, N.; Pityana, S.; Adeosun, S.; Aramide, O.; Lengopeng, T. Process Optimization of High Entropy Alloys by Laser Additive Manufacturing. *Eng. Rep.* **2020**, *2*, e12252. [CrossRef]

16. Chew, Y.; Zhu, Z.G.; Weng, F.; Gao, S.B.; Ng, F.L.; Lee, B.Y.; Bi, G.J. Microstructure and Mechanical Behavior of Laser Aided Additive Manufactured Low Carbon Interstitial Fe49.5Mn30Co10Cr10C0.5 Multicomponent Alloy. *J. Mater. Sci. Technol.* **2021**, *77*, 38–46. [CrossRef]
17. Yeh, J.W.; Chen, S.K.; Lin, S.J.; Gan, J.Y.; Chin, T.S.; Shun, T.T.; Tsau, C.H.; Chang, S.Y. Nanostructured High-Entropy Alloys with Multiple Principal Elements: Novel Alloy Design Concepts and Outcomes. *Adv. Eng. Mater.* **2004**, *6*, 299–303. [CrossRef]
18. Cantor, B.; Chang, I.T.H.; Knight, P.; Vincent, A.J.B. Microstructural Development in Equiatomic Multicomponent Alloys. *Mater. Sci. Eng. A* **2004**, *375–377*, 213–218. [CrossRef]
19. Guo, S.; Liu, C.T. Phase Stability in High Entropy Alloys: Formation of Solid-Solution Phase or Amorphous Phase. *Prog. Nat. Sci. Mater. Int.* **2011**, *21*, 433–446. [CrossRef]
20. Miracle, D.B.; Senkov, O.N. A Critical Review of High Entropy Alloys and Related Concepts. *Acta Mater.* **2017**, *122*, 448–511. [CrossRef]
21. Ince, F.D.; Özel, T. Laser Surface Texturing of Materials for Surface Functionalization: A Holistic Review. *Surf. Coat. Technol.* **2025**, *498*, 131818. [CrossRef]
22. De Palo, R.; Emanuele Mazzarone, A.; Volpe, A.; Gaudiuso, C.; Paolo Mezzapesa, F.; Spagnolo, V.; Ancona, A. Investigation of Laser-Induced Surface Structures (LIPSS) on Quartz and Evaluation of Their Influence on Material Wettability. *Opt. Laser Technol.* **2024**, *169*, 110097. [CrossRef]
23. Wood, M.J.; Servio, P.; Kietzig, A.M. The Tuning of Lipss Wettability during Laser Machining and through Post-Processing. *Nanomaterials* **2021**, *11*, 973. [CrossRef] [PubMed]
24. Bonse, J.; Koter, R.; Hartelt, M.; Spaltmann, D.; Pentzien, S.; Höhm, S.; Rosenfeld, A.; Krüger, J. Tribological Performance of Femtosecond Laser-Induced Periodic Surface Structures on Titanium and a High Toughness Bearing Steel. *Appl. Surf. Sci.* **2015**, *336*, 21–27. [CrossRef]
25. Murzin, S.P.; Balyakin, V.B.; Liedl, G.; Melnikov, A.A.; Fürbacher, R. Improving Tribological Properties of Stainless Steel Surfaces by Femtosecond Laser Irradiation. *Coatings* **2020**, *10*, 606. [CrossRef]
26. Voisiat, B.; Wang, W.; Holzhey, M.; Lasagni, A.F. Improving the Homogeneity of Diffraction Based Colours by Fabricating Periodic Patterns with Gradient Spatial Period Using Direct Laser Interference Patterning. *Sci. Rep.* **2019**, *9*, 7801. [CrossRef]
27. Kiel, F.; Trinschek, S.; Kuchmizhak, A.; Gurevich, E.L. Colouration of Diamond Surfaces by Laser-Induced Periodic Surface Structuring. *Opt. Laser Technol.* **2024**, *168*, 109882. [CrossRef]
28. Hareancz, F.; Juhász, G.; Windisch, M.; Heczel, A.; Vida, Á. Preparation of High Entropy Alloys Without Pre-Alloying, Using Laser Melt Deposition (LMD) Technique. *Coatings* **2025**, *15*, 116. [CrossRef]
29. Shao, G.; Lei, J.; Zhang, F.; Wang, S.; Hu, H.; Wang, K.; Tan, P.; Yi, J. A Study of the Microstructure and Mechanical and Electrochemical Properties of CoCrFeNi High-Entropy Alloys Additive-Manufactured Using Laser Metal Deposition. *Coatings* **2023**, *13*, 1583. [CrossRef]
30. Huang, A.; Liu, Y.; Liu, J.; Yang, S.; Huang, J. Optimization of Process Parameters for Laser Cladding of AlCoCrFeNi High-Entropy Alloy Coating Based on the Taguchi-Grey Relational Analysis. *Materials* **2025**, *18*, 4463. [CrossRef]
31. Nelson, J.B.; Riley, D.P. An Experimental Investigation of Extrapolation Methods in the Derivation of Accurate Unit-Cell Dimensions of Crystals. *Proc. Phys. Soc.* **1945**, *57*, 160. [CrossRef]
32. Yuan, Y.; Li, H.; Xu, X. Formation of Dual-Phase Structure and Property Enhancement Mechanism in Deep Undercooling Solidification of CoCrFeNi High-Entropy Alloy. *J. Alloys Compd.* **2025**, *1040*, 183659. [CrossRef]
33. Gorban, V.F.; Krapivka, M.O.; Myslyvchenko, O.M. Formation Conditions and Properties of High-Entropy Alloys Creating σ-Phase. *Mater. Sci.* **2024**, *59*, 770–775. [CrossRef]